Statistical analysis of E-jet print parameter effects on Ag-nanoparticle ink droplet size

Statistical analysis of E-jet print parameter effects on Ag-nanoparticle ink droplet size

M-M. Laurila, B. Khorramdel, A. Dastpak and M. Mäntysalo

Laboratory of Electronics and Communications Engineering, Tampere University of Technology, Tampere, 33720, Finland

Email: mika-matti.laurila@tut.fi

Abstract. In this paper, we have studied the print parameter effects on electrohydrodynamic inkjet (E-jet) resolution using statistical analysis. In order to make the E-jet manufacturing process feasible, the effect of printing parameters on the ejected droplet size must be modelled and optimized. To this end, there exist two approaches: parameter effects can be modelled using theoretical calculations or they can be generated directly from empirical data using statistical analysis. The first option has been explored by multiple research groups, whereas the latter has received less interest. In this article, the effect of printing parameters on width of AC-pulsed E-jet deposited Ag-nanoparticle ink droplets are investigated using design of experiments (DoE) approach and statistical analysis. As a result, a statistical model for deposited droplet width is generated using four print parameters (print height, bias voltage, peak voltage and frequency) as predictors. The model can predict 94.24% of the measured width variation with a standard deviation of 1.05 µm.

1. Introduction

It has been demonstrated that the electrohydrodynamic inkjet (E-jet) printers are capable of producing patterns with micron scale feature sizes [1]. This attribute makes E-jet printing an interesting alternative for driving the device miniaturization in the field of printed electronics. Potential applications can be found for example in fabrication of miniaturized thin-film transistors [1], memristors [2] and sensor devices on flexible and stretchable substrates [3][4] or in integration of additive fabrication technologies to electronics packaging, where high density interconnects (e.g. TSV's [5], UBM [6] and RDL's [7]) are required to redistribute the signal paths from chip to PCB. Unrelated to electronics fabrication, the E-jet can be also used in biotechnology for compartmentalization of biomolecular samples [8] and patterning of polymeric scaffolds for tissue engineering [9]. In order to make these fabrication processes feasible, it is vital to be able to control the print resolution which, in turn, is mainly controlled by the size of the deposited droplets.

Previously, the effect of different process parameters on E-jet behavior have been studied by various research groups starting from early articles on jetting modes of constant voltage EHD electrospray devices by Cloupeau and Prunet-Foch [10]. More lately, Seongpil et al found that frequency of droplet ejection in AC modulated E-jet printer depends not only on frequency of the voltage, but also on viscosity and electrical conductivity of the ink [11], whereas Mishra et al concluded that size of the deposited droplets can be controlled by varying the voltage pulse length [12]. In addition, J. Park et al predicted dimensions of printed patterns by using theoretical formulas with substrate surface wettability, ink flow rate, printing speed, voltage pulse frequency and pulse length as variables [13]. Also, the effect of solvent and solid weight percent of a nanoparticle based

ink has been investigated by Kang et al [14] whereas Choi et al found that the nozzle diameter will affect the volume of the deposited droplets [15]. The effects of pulse- and bias-voltages on the jetting have been studied by Li et al [16].

Theoretical modelling of parameter effects provides fundamental insight into E-jet operation, but is not necessarily enough for manufacturing environment where importance is on the repeatability and reproducibility of the fabrication process. In this article, we have quantified these aspects via statistical modelling of the print process. Specifically, we have used design of experiments (DoE) approach and analysis of variance (ANOVA) for the DoE results to generate a numerical model between the width of the printed droplets and frequency, print height, peak and bias voltage. Additional advantage of this approach is that contrary to the one-variable-at-a-time approach used in the aforementioned studies, it can also estimate the interactive effects between variables and easily detect the parameters with strongest effect.

2. Materials and methods

2.1 Electrohydrodynamic inkjet (E-jet)

The deposition tool used in this study is a commercially available E-jet printer Super Inkjet SIJ-S050 developed by SIJ Technology Inc., Tsukuba, Japan. The print head consists of a hollow glass needle (nozzle) which has a narrow diameter capillary opening at the bottom end; at the same time the nozzle acts as an ink chamber. During operation, the ink is charged using a charging electrode whereby a potential difference between the ink meniscus and grounded xy-stage is generated. A jet of ink is pulled out when the strength of the electric field between the meniscus and the substrate exceeds a threshold value. During operation, the strength of the electric field can be varied by varying the nozzle-to-substrate distance (d), or the bias (V_{bias}) and peak voltage (V_{max}) of the voltage pulse. It is also possible to control the pulse frequency (f) and speed of the xy-stage (v). The movement of the xy-stage determines the geometry of the printed pattern.

Super Fine Nozzle (SIJ Technology Inc.) with the smallest diameter capillary of the three available options was used for the experiments.

2.2 Nanoparticle ink

The ink used in this study is a commercial Ag-nanoparticle ink DGP 40TE-20C (Advanced Nanoproducts Co. Ltd., Korea) optimized for conventional inkjets. The ink specifications are presented in Table 1.

Table 1: *ANP DGP 40TE-20C ink specifications* [17]

Parameter	**Value**
Solid material	Ag
Solvent	Triethylene glycol monoethyl ether
Solid content	30-35 wt%
Sintering	190°C for 60 min
Resistivity	5-9 µOhm·cm
Viscosity	10-17 mPas·s

2.3 Substrate

The substrate was 675 µm thick silicon wafer covered with 1.4 µm oxide layer and 0.1 µm titanium-tungsten (Ti/W) layer on top. Since the Ti/W-layer is conductive, charge accumulation should not happen during printing and this should improve the stability of jetting [18]. To further ensure that there is no charge accumulation, a copper tape was used to connect the top of the wafer to the grounded xy-stage. The substrate was wiped with isopropyl alcohol before printing.

2.4 Measurement and analysis tools

The width measurements were performed with Olympus BX51 optical microscope using a 100X objective and QuickPhoto Camera 2.1 imaging software. Measurement system analysis (Supplementary Information 1) showed that the measurement equipment related variation accounts for 0.84 µm of the detected total variation.

Minitab 17 statistical software was used for measurement system analysis and generating the experimental design and response surface regression for the measurement data.

3. Design of experiments

3.1 Parameter screening

The print resolution in E-jet printers is controlled by varying the volume of ejected ink during each voltage pulse. This creates the basis for controlling dimensions and quality of any inkjet printed feature be it a conductor, bump or pillar. For example, according to Soltman et al. [19], when the droplet spacing is smaller than the droplet diameter on the substrate, the width of an inkjet printed line can be predicted by:

$$W = 2 * \sqrt{\frac{2V_{drop}}{\pi * \Delta x * f(\theta)}} \quad (1)$$

where W is the width of the printed line, V_{drop} the ejected volume of liquid during the pulse, Δx the drop spacing on the substrate and $f(\theta)$ the correction factor which depends on the wetting angle of the ink [19]; Δx is a function of frequency and printing speed whereas $f(\theta)$ can be experimentally determined for different ink/substrate combinations.

In E-jet printers, V_{drop} depends on the strength of the electric field (E) acting on the ink meniscus [1]. The field strength is increased by introducing higher charging voltage (bias voltage V_{bias} or peak voltage V_{max}) or decreasing the distance between the nozzle and substrate (h):

$$V_{drop} \propto E = \frac{V_{bias} + V_{max}}{h} \quad (2)$$

However, V_{drop} is also proportional to the pulse width (T_p) which, in case of a square wave, depends on the duty cycle (d) and frequency (f) of the pulse [12]:

$$V_{drop} \propto T_p = \frac{d}{f} \quad (3)$$

For the sine waveform used in this study, V_{drop} should be therefore proportional to the cycle time (T_C) of the pulse:

$$V_{drop} \propto T_C = \frac{1}{f} \quad (4)$$

The nozzle parameters (e.g. diameter) and ink parameters (e.g. conductivity, viscosity, surface tension) will also affect the V_{drop}. Because these can not be varied during the printer operation, they are considered as constant parameters similar to substrate surface energy, temperature and humidity.

The remaining print parameters which can be easily varied during print process are V_{bias}, V_{max}, h and f. These were included as factors in the experimental design.

3.3 Response surface design

A Box-Behnken response surface design (BBD) was chosen so that the possible quadratic effects could be included in the model. The BBD consists of experimental points at the edges of the design space with additional experimental points at the center i.e. three levels for each factor. The design was separated into three experimental blocks and the whole design was replicated once in order to increase the reliability of the model. With the replicate, the total number of runs was 54. The width of the deposited droplets was used as response [20].

During the experiment, it was noted that the factor *h* has extra variation depending on the block due to substrate tilt in vertical direction. This variation was measured and the factor levels adjusted accordingly leading to more than three levels for the *h*. The experimental points in coded coefficients and corresponding factor levels are shown in Table 2. Complete list of all the runs and measurements are presented in Supplementary Information 2.

Table 2: *Parameters included in the experimental design and the experimental points in coded coefficients with respective factor levels. During the experiment, room temperature was 21.0 C and relative humidity 26%.*

Parameter	-1	0	1	Unit
V_{max}	220	235	250	Volt
V_{bias}	0	15	30	Volt
f	50	60	70	Hertz
h	28	50	71	µm

Depending on the print parameters, ink may be ejected only on the positive/negative side of the pulse, or on both sides. However, measurements were performed only for the droplets ejected during the positive pulse cycle since it was noted that this is not affected by droplet ejection during negative cycle. This effect is apparent from Figure 1, which presents the overall view of the fourth block and higher magnification images of runs 32 and 33. The negative peak voltage of run 32 is 30 V lower compared to run 33 (-220 V vs. -190 V) resulting in droplet ejection during the negative cycle as well, but the positive cycles result in approximately same amount of ink since the positive peak voltages are identical (250 V vs. 250 V).

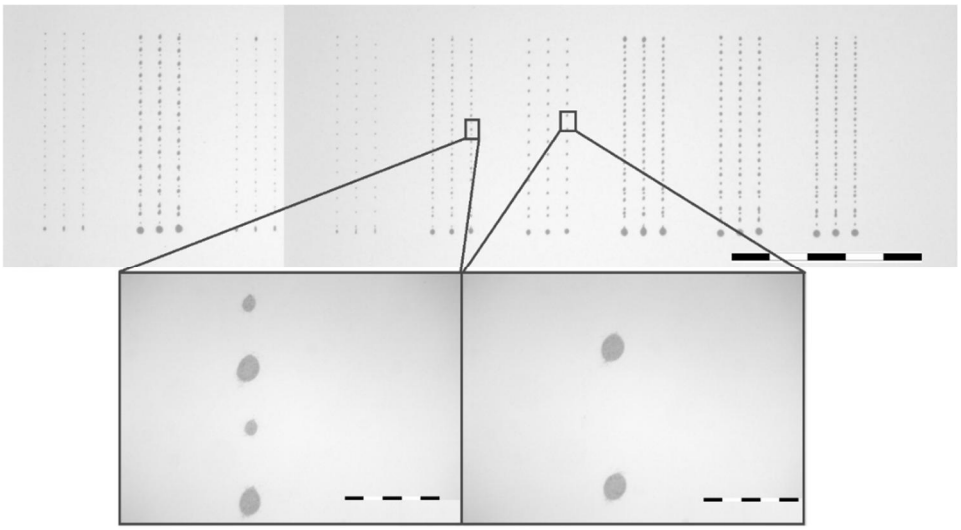

Figure 1: *Upper picture shows the fourth block (5X magnification) and lower, high magnification (100X) images show the runs 32 and 33. The scale bar in upper image is 1 mm and in lower images 50 µm.*

4. Statistical model

Analysis of variance (ANOVA) was performed for the measurement data to assess the statistical significance of the chosen factors. First, the statistically significant factors were separated from the insignificant ones using backwards elimination and P-value smaller than 0.01 as criterion; this indicates at least 99% confidence rate that the decision to include the effect in the model is correct. Table 3 shows the ANOVA results after removing the insignificant factors. In Table 3 DF denotes degrees of freedom, Adj. SS the adjacent sum of squares, Adj. MS the adjacent mean sum of squares, F-value indicates the strength of the effect and P-value the aforementioned statistical significance. VIF is the variance inflation factor used to detect multicollinearity between factors.

Table 3: *Analysis of variance*

Source	DF	Adj. SS	Adj. MS	F-value	P-value	VIF
Model	10	739.814	73.981	66.94	0.000	
Blocks	5	5.173	1.035	0.94	0.468	
Linear	4	641.178	160.295	145.04	0.000	
$\boldsymbol{V_{max}}$	1	355.177	355.177	321.38	0.000	1.01
$\boldsymbol{V_{bias}}$	1	37.374	37.374	33.82	0.000	1.00
f	1	17.389	17.389	15.73	0.000	1.01
h	1	268.472	268.472	242.92	0.000	1.16
Square	1	67.422	67.422	61.01	0.000	
$\boldsymbol{V_{bias} * V_{bias}}$	1	67.422	67.422	61.01	0.000	1.16
Error	41	45.312	1.105			
Total	51	785.126				

The ANOVA results show that the experimental blocks have P-values >> 0.01, which indicates that the blocks themselves are statistically insignificant, as they should be. The VIF-values near unity show that there is no multicollinearity between the factors. This indicates that the adjustment of factor h after the experiment did not affect the precision of the statistical model. As for the factor effects, the F-values show that V_{max} is the strongest one followed by h, the quadratic term of V_{bias}, V_{bias} and f. The effects are illustrated in Figure 2,

which shows the response surfaces of all the factor combinations. From this figure, it can be also seen that the effect of *f* and *h* are negative i.e. increasing them decreases the width of the deposited droplets.

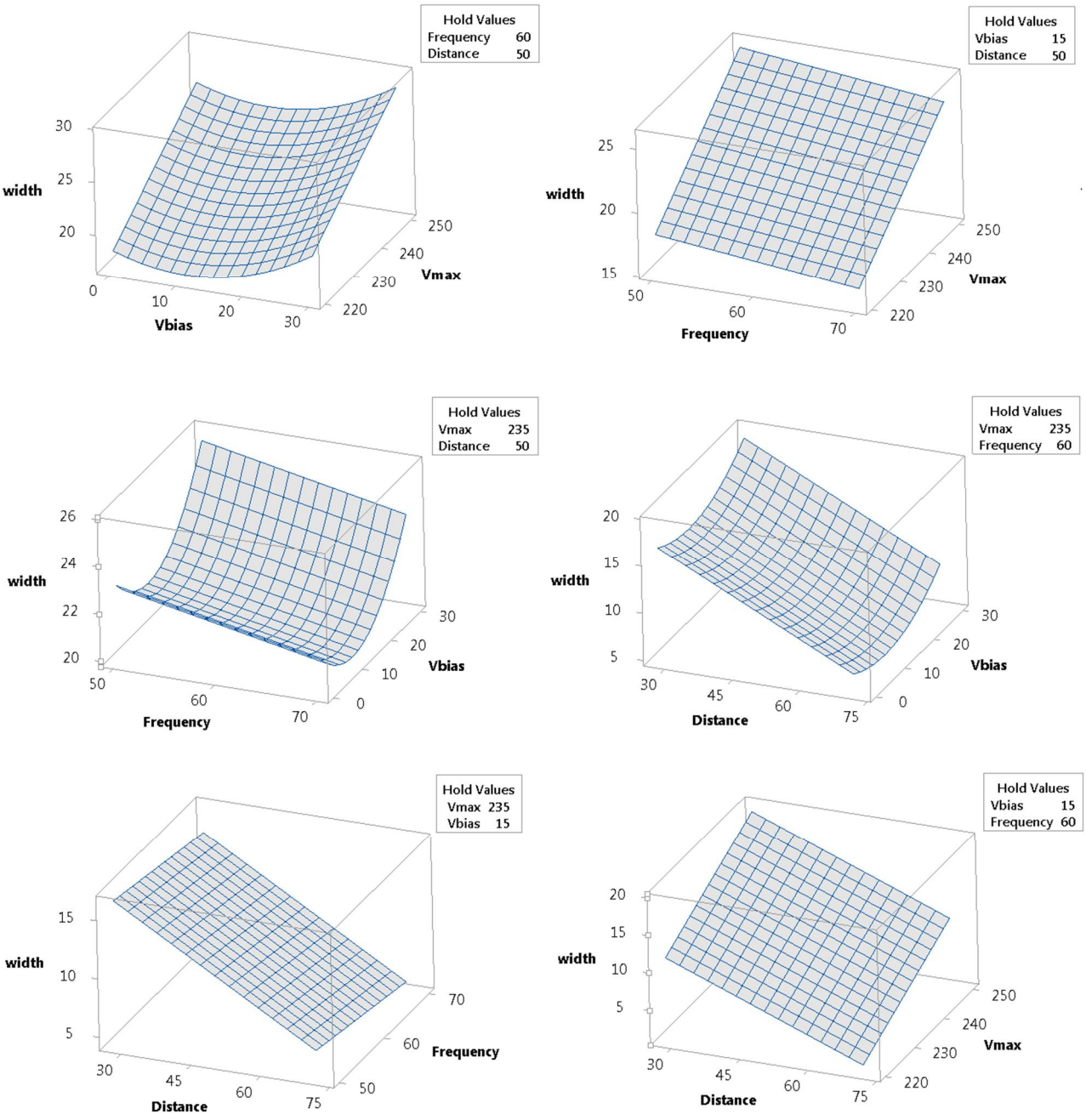

Figure 2: *Response surface plots for different factor combinations. The width and distance (h) are in micrometers, the* $\boldsymbol{V_{max}}$ *and* $\boldsymbol{V_{bias}}$ *in Volts, and frequency (f) in Hertz.*

Expressed in numerical form, the response surface regression model is:

$$width = -33.43 + 0.2632 * V_{max} - 0.2226 * V_{bias} - 0.0873 * f - 0.2353 * h + 0.01019\, V_{bias}^{2} \qquad (5)$$

where V_{max} and V_{bias} are expressed in Volts, *f* in Hertz and *h* in micrometers. According to the R-squared value, this model explains 94.24% of the detected variation with a standard deviation of 1.05 µm. The value is

very good considering the measurement system variation of 0.84 µm determined in the measurement system analysis. The model validity was checked using residual plots presented in Supplementary Information 1.

The model can be adjusted for substrates with different surface energy by printing a set of droplets with random print parameters, measuring the droplet width, and adjusting the first coefficient of equation (5) accordingly. After this, the print resolution can be predicted by using the adjusted equation.

5. Analysis

Since the statistical model is based on purely numerical analysis, it does not take account of physical restrictions (such as minimum width limit of zero micrometers) and is therefore only applicable within the design space defined by the minimum/maximum factor levels used in the experiment. Within this design space, the model predicts that V_{max} has the strongest effect followed by *h*, the quadratic term of V_{bias}, V_{bias} and *f*.

The difference in the strength of the effects of the voltage terms V_{max} and V_{bias} can be seen for example in runs 13 and 18 shown in Figure 3. The print height, frequency and total voltage ($V_{tot} = V_{bias} + V_{max}$) are the same in both runs, but the V_{max} and V_{bias} differ (see inset of figure). According to [16] the changes in V_{max} and V_{bias} affect the electric field distribution differently: while the V_{max} mainly modulates the electric field tangential to the meniscus surface, the V_{bias} affects the electric field normal to the meniscus surface. The resulting jetting behavior is therefore different. For thorough study of effects of electric field components on E-jet jetting behavior, the reader is suggested to turn to references [16] and [21].

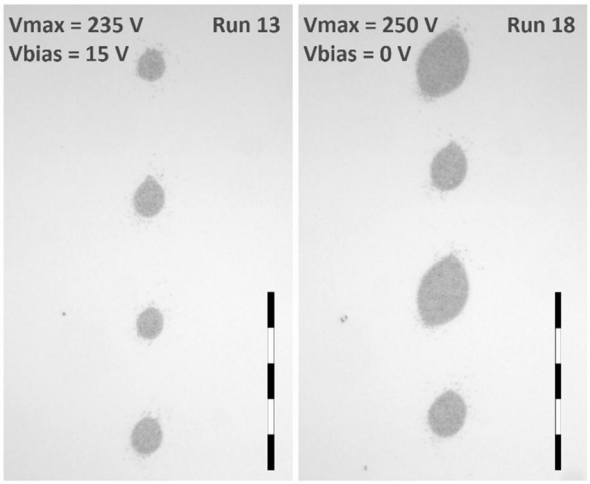

Figure 3: *Confirmation runs printed with and without* $\boldsymbol{V_{bias}}$*. Printing speed varied between runs. Scale bar is 50 µm.*

The negative relationship between *h* and width of the deposited droplets can be understood by recalling the definition of electric field strength (equation 2) which decreases as *h* is increased. The same relationship also explains why the V_{max} and V_{bias} have positive relationship with the width of the deposited droplets.

The negative effect of *f* can be understood by recalling the equation (4) which states that decreasing cycle time decreases the volume of ejected ink. When the frequency is increased, the cycle time will decrease accordingly thereby leading to a negative relationship between frequency and droplet width.

In order to validate the model, four confirmation runs with target widths of 7.5 µm, 10 µm, 12.5 µm and 15 µm were printed using three different nozzles. The runs were performed with constant print heights of 50 µm and 70 µm in order to simulate real manufacturing environment. Furthermore, V_{bias} was kept constant at 30 V in order to suppress the ejection during the negative cycle of the pulse. Using these constraints, equation (8) was solved with the Minitab response optimizer tool. Images in Figure 3 show the confirmation runs for 7.5 µm and 12.5 µm target widths for Nozzle 2.

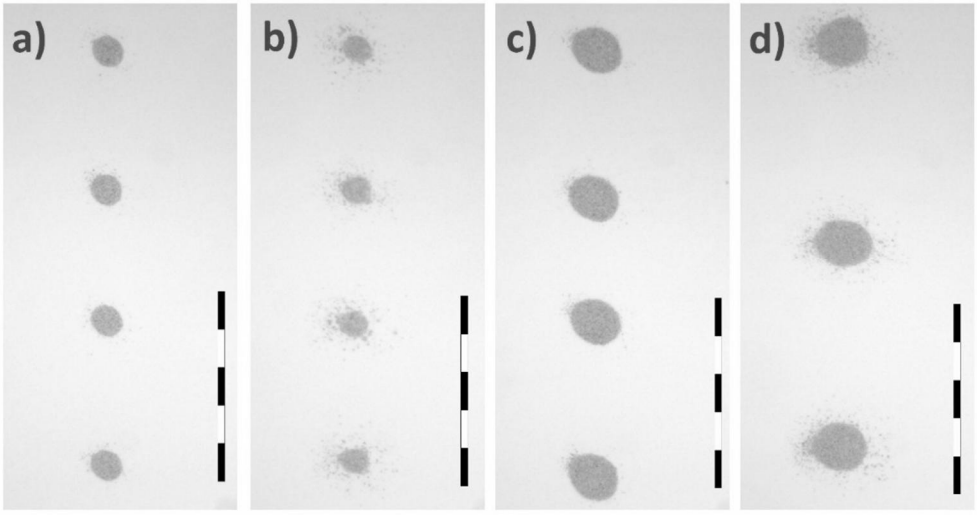

Figure 3: *Confirmation runs for Nozzle2 with target widths of 7.5µm (a and b) and 12.5µm (c and d). The print height in a) and c) is 50 µm and in b) and d) 70 µm. Lower print height seems to produce more uniform droplets. Scale bar is 50 µm.*

Table 4: *Droplet widths for confirmation runs. The room temperature was 20.0 C and relative humidity 28 %.*

	Target (95% conf. int.)	**7.5 µm** (6.5; 8.5)	**10 µm** (9.0;11.0)	**12.5 µm** (11.5; 13.5)	**15 µm** (14.0; 16.0)
h = 50µm	Nozzle1	7.8 µm	9.3 µm	12.9 µm	15.7 µm
	Nozzle2	8.0 µm	9.3 µm	12.9 µm	15.8 µm
	Nozzle3	5.3 µm	7.0 µm	11.6 µm	13.5 µm
h = 70µm	Nozzle1	7.7 µm	10.7 µm	14.5 µm	16.6 µm
	Nozzle2	7.9 µm	10.3 µm	14.3 µm	17.2 µm
	Nozzle3	5.9 µm	8.2 µm	12.9 µm	15.8 µm

Based on Figure 3 and Table 4, it is preferable to use lower print height since this produces droplets with less edge roughness and increases the prediction accuracy of the regression model. For Nozzle1 and Nozzle2 and 50 µm print height, all the droplets are within the 95% confidence interval compared to only 50% for 70 µm print height.

The categorically smaller widths produced by the Nozzle3 are likely related to the nozzle filling process. According to Lee et al. [21], the three forces balancing the ink meniscus at the tip of the nozzle are the hydrostatic force (F_H) which supplies ink to the meniscus, the surface tension which keeps the meniscus attached to the glass capillary (F_C) and the electrostatic force which pulls the meniscus downwards (F_E). While there should not be any change in F_E between the DoE and confirmation runs, or the F_C since the same nozzle type and ink was used, the F_H may vary since the ink level inside the nozzle may differ between different filling times. In the case of Nozzle3, lower filling level should reduce the hydrostatic pressure and the F_H thereby decreasing the size of the jetted droplets. In the manufacturing process, this deviation can be corrected by measuring the droplet width and adjusting the coefficients of equation (4) accordingly.

6. Conclusion

A statistical model was generated to relate the width of the deposited droplets to the four main print parameters.

The peak voltage has the strongest effect on the droplet size followed by print height, DC-voltage and frequency. The R-squared value of the model was 94.24% with standard deviation of 1.05 µm. The statistical model applies for droplet diameters between 3.5 µm to 21 µm. Furthermore, it was noted that smaller print height suppresses the spray around the droplets.

Acknowledgements
This work is supported by ENIAC-JU Project Prominent grant No. 324189 and Tekes grant No. 40336/12.

M. Mäntysalo is supported by Academy of Finland grant No. 288945.

Furthermore, the authors would like to thank Silex Ab, Sweden, and especially M.Sc. Jessica Liljeholm, for providing the Ti/W-covered silicon wafers.

References

[1] Park J-U, Hardy M, Kang S J, Barton K, Adair K, Mukhopadhyay D K, Lee C Y, Strano M S, Alleyne A G, Georgiadis J G, Ferreira P M and Rogers J A 2007 High-resolution electrohydrodynamic jet printing *Nat Mater* **6** 782–9

[2] Duraisamy N, Malik N, Kim H, Jo J and Choi K 2012 Fabrication of TiO2 thin film memristor device using electrohydrodynamic inkjet printing *Thin Solid Films* **520** 5070–4

[3] Onses M S, Sutanto E, Ferreira P M and Alleyne A G 2015 Mechanisms, capabilities, and applications of electrohydrodynamic jet printing *Small* **11** 4237-66

[4] Vuorinen T, Laurila M, Mangayil R, Karp M and Mäntysalo M High resolution E-jet printed temperature sensor on bacterial nanocellulose substrate, *EMBEC Conf.* **2017-June** *In press*

[5] Khorramdel B, Laurila M M and Mäntysalo M 2015 Metallization of high density TSVs using super inkjet technology *Proc. - Electron. Components Technol. Conf.* **2015**–**July** 41–5

[6] Khorramdel B, Liljeholm J, Laurila M M, Lammi T, Mårtenson G, Ebefors T, Niklaus F and Mäntysalo M 2017 Inkjet printing technology for increasing the I/O density of 3D TSV interposers, *Microsyst. and Nanoengin.* **3** *17002*

[7] Laurila M M, Soltani A and Mäntysalo M 2015 Inkjet printed single layer high-density circuitry for a MEMS device *Proc. - Electron. Components Technol. Conf.* **2015**–**July** 968–72

[8] Sharma B, Takamura Y, Shimoda T and Biyani M 2016 A bulk sub-femtoliter in vitro compartmentalization system using super-fine electrosprays *Sci. Rep.* **6** 26257

[9] Wei C and Dong J 2014 Hybrid hierarchical fabrication of three-dimensional scaffolds *J. Manuf. Process.* **16** 257–63

[10] Cloupeau M and Prunet-Foch B 1990 Electrostatic spraying of liquids: Main functioning modes *J. Electrostat.* **25** 165–84

[11] An S, Lee M W, Kim N Y, Lee C, Al-Deyab S S, James S C and Yoon S S 2014 Effect of viscosity, electrical conductivity, and surface tension on direct-current-pulsed drop-on-demand electrohydrodynamic printing frequency *Appl. Phys. Lett.* **105** *214102*

[12] Mishra S, Barton K L, Alleyne A G, Ferreira P M and Rogers J A 2010 High-speed and drop-on-demand printing with a pulsed electrohydrodynamic jet *J. Micromechanics Microengineering* **20** 95026

[13] Park J, Kim B, Kim S Y and Hwang J 2014 Prediction of drop-on-demand (DOD) pattern size in pulse voltage-applied electrohydrodynamic (EHD) jet printing of Ag colloid ink *Appl. Phys. A Mater. Sci. Process.* **117** 2225–34

[14] Kang D K, Lee M W, Kim H Y, James S C and Yoon S S 2011 Electrohydrodynamic pulsed-inkjet characteristics of various inks containing aluminum particles *J. Aerosol Sci.* **42** 621–30

[15] Choi H K, Park J U, Park O O, Ferreira P M, Georgiadis J G and Rogers J A 2008 Scaling laws for jet pulsations associated with high-resolution electrohydrodynamic printing *Appl. Phys. Lett.* **92** 2006–9

[16] Li J L 2006 On the meniscus deformation when the pulsed voltage is applied *J. Electrostat.* **64** 44–52

[17] Advanced Nano Products Ltd., 'ANP Silverjet datasheet' [Online] Available: http://anapro.com/eng/product/silver_inkjet_ink.html.

[18] Wei C, Qin H, Ramirez-Iglesias N A, Chiu C-P, Lee Y-S and Dong J 2014 High-resolution ac-pulse modulated electrohydrodynamic jet printing on highly insulating substrates *J. Micromechanics Microengineering* **24** 45010

[19] Soltman D and Subramanian V 2008 Inkjet-printed line morphologies and temperature control of the coffee ring effect *Langmuir* **24** 2224–31

[20] Bezerra M A, Santelli R E, Oliveira E P, Villar L S and Escaleira L A 2008 Response surface methodology (RSM) as a tool for optimization in analytical chemistry *Talanta* **76** 965–77

[21] Lee A, Jin H, Dang H W, Choi K H and Ahn K H 2013 Optimization of experimental parameters to determine the jetting regimes in electrohydrodynamic printing *Langmuir* **29** 13630–9